

# High Resolution Dynamic-Susceptibility Contrast Perfusion Imaging Using Multi-Echo Parallel EPI

T. H. Jochimsen<sup>1</sup>, R. Newbould<sup>1</sup>, S. Skare<sup>1</sup>, D. B. Clayton<sup>1</sup>, M. E. Moseley<sup>1</sup>, R. Bammer<sup>1</sup>

<sup>1</sup>Lucas MRS/I Center, Stanford University, Palo Alto, CA, United States

## Introduction

In dynamic-susceptibility contrast-based magnetic resonance imaging (DSC-MRI), time series are acquired during the first pass of an intravascular tracer. From these dynamic scans, it is possible to estimate cerebral blood volume (CBV). Furthermore, from pixel-wise deconvolution with an arterial input function (AIF) yields maps of cerebral blood flow (CBF) and mean transit time (MTT) [1, 2]. There are several benefits of using a multi-echo (ME) approach for DSC-MRI [3-5]: 1)  $\Delta R_2^*$ , which is assumed to be proportional to tracer concentration, can be measured undisturbed from  $T_1$  enhancement caused by the tracer (e.g. in the presence of a blood-brain-barrier disruption). 2) Without the need for a pre-bolus baseline signal, the method becomes less sensitive to large-scale signal instabilities and patient motion. 3) Automatic selection of arterial input function [6, 7] can be based on the first echo which has the appropriate dynamic range (high tracer concentration) and the least artifacts (signal voids). 4) If the dynamic range using  $\Delta R_2^*$  of all echoes is too small to estimate the AIF in arterial voxels because of a large signal drop, the procedure can be limited to the first echo(es) [5], for example by a magnitude-weighted exponential fit.

In combination with parallel imaging (PI), a high spatial and temporal resolution can be achieved [8]. In addition, PI reduces image artifacts related to EPI. We will refer to this technique, i.e. the combination of ME with PI, as PERfusion with Multiple Echoes and Temporal Enhancement (PERMEATE).

## Materials and Methods

All scans were performed on a 1.5 T scanner (Signa LX/i, GE Medical Systems, Waukesha, WI) fitted with high performance gradients (maximum strength: 50 mT/m, rise time: 270  $\mu$ s). PI was performed by means of an eight-element coil together with 2 different reduction factors:  $R=3$  and  $R=4$ . A multi-echo multi-slice gradient-echo EPI sequence was implemented to image 15 slices (5-mm thickness, 1-mm gap) with 240-mm FOV and a matrix size  $96 \times 96$ . The number of echoes equals the reduction factor. Sequence parameters were:  $TE = 13.8, 31.6, 49.4$  ms ( $R=3$ ) and  $TE = 12.4, 27.3, 42.2, 57.1$  ms ( $R=4$ ), 100 repetitions with  $TR = 1225$  ms,  $\pm 100$  kHz receiver bandwidth and a flip angle of  $70^\circ$ . Image reconstruction was performed by a GRAPPA-based algorithm [9]. A single dose of 0.1 mmol/kg Gd-DTPA was administered at a rate of 4 ml/s followed by 20-ml saline flush. After converting signal magnitudes to  $\Delta R_2^*$  time series, perfusion maps were calculated by a block-circulant singular-value decomposition for tracer arrival timing-insensitive deconvolution [10] with a tolerance threshold  $p_{\text{SVD}} = 10\%$  using an automatically selected AIF [7] from the first echo. As a measure of accuracy of the method, the ratio of CBF and CBV between gray and white matter was estimated by values within manually drawn regions-of-interest.

## Results

As an example, Fig. 1 displays perfusion maps of a healthy volunteer obtained by PERMEATE. Gray and white matter can be very well delineated. The AIFs shown in Fig. 2 demonstrate that the first echo has the most appropriate dynamic range for AIF selection and was hence used for further CBV/CBF analysis. Gray/white matter ratios of two subjects are shown in Table 1. The values and their age-dependency are in good agreement with previously reported values [1].

## Discussion and Conclusions

PERMEATE allows robust, accurate, and distortion-reduced high-resolution estimation of  $\Delta R_2^*$  and the AIF which is the basis for CBV/CBF calculation. It can be expected that, due to the advantages of ME acquisition mentioned above, quantitative CBF and CBV calculations become more accurate.

## Acknowledgements

This work was supported in part by the NIH (1R01EB002771), the Center of Advanced MR Technology at Stanford (P41RR09784), Lucas Foundation, and Oak Foundation.

## References

- [1] Rempp KA, et al. 193(1994):637. [2] Østergaard L, et al. *Magn Reson Med*, 36(1996):715. [3] Kuperman VY, et al. *J Magn Reson Imag*, 6(1996):765. [4] Miyati T, et al. *J Magn Reson Imag*, 7(1997):231. [5] Vonken EA, et al. *J Magn Reson Imag*, 10(1999):109. [6] Carroll TJ, et al. *Radiology*, 227(2003):593. [7] Mlynash M, et al. *Am J Neuroradiol*, 26(2005):1479. [8] Larkman DJ, et al. *J Magn Reson Imag*, 14(2001):329. [9] Skare S, et al. *ISMRM*, 13(2005):2422. [10] Wu O, et al. *Magn Reson Med*, 50(2003):164.

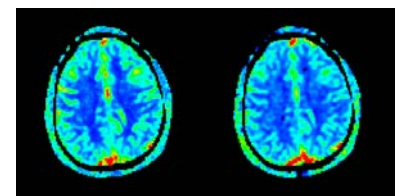


Figure 1: CBF (left) and CBV (right) maps of a 32-year old healthy volunteer, acquired with  $R = 4$ .

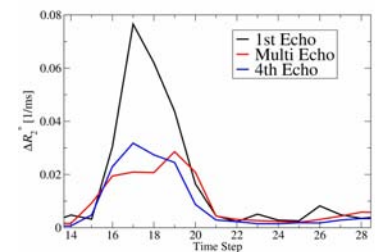


Figure 2: AIF obtained from 1st echo, 4th echo and by multi-echo fit ( $R = 4$ ).

| $R$ | Age (y) | $\text{CBF}_{\text{GM}}/\text{CBF}_{\text{WM}}$ | $\text{CBV}_{\text{GM}}/\text{CBV}_{\text{WM}}$ |
|-----|---------|---|---|
| 4   | 32      | $2.8 \pm 0.5$                                   | $2.9 \pm 0.3$                                   |
| 3   | 32      | $3.0 \pm 0.5$                                   | $3.3 \pm 0.7$                                   |
| 4   | 50      | $2.4 \pm 0.2$                                   | $2.5 \pm 0.3$                                   |

Table 1: Gray/white matter ratios of CBF and CBV in two different healthy volunteers of